Biointerphases
A Journal of Biomaterials and Biological Interfaces

Functional nanothin films plasma-deposited from 2-isopropenyl-2-oxazoline for biosensor applications

Cite as: Biointerphases **15**, 051005 (2020); https://doi.org/10.1116/6.0000499
Submitted: 29 July 2020 . Accepted: 01 September 2020 . Published Online: 24 September 2020

Kit Man Chan, Cherine Amoura, Amelia Whiteley, Julien Rouget, Hanieh Safizadeh Shirazi, Alex Cavallaro, Krasimir Vasilev, and Melanie MacGregor

Biointerphases
A Journal of Biomaterials and Biological Interfaces

ARTICLE

avs.scitation.org/journal/bip

Functional nanothin films plasma-deposited from 2-isopropenyl-2-oxazoline for biosensor applications

Cite as: Biointerphases 15, 051005 (2020); doi: 10.1116/6.0000499
Submitted: 29 July 2020 · Accepted: 1 September 2020 ·
Published Online: 24 September 2020

Kit Man Chan,[1] Cherine Amoura,[2] Amelia Whiteley,[3] Julien Rouget,[3] Hanieh Safizadeh Shirazi,[1] Alex Cavallaro,[4] Krasimir Vasilev,[1,4] and Melanie MacGregor[1,4,a)]

AFFILIATIONS

[1]School of Engineering, UniSA STEM, University of South Australia, Mawson Lakes, South Australia 5095, Australia
[2]Faculty of Science and Technology, University of Nantes, 2 Chemin de la Houssinière, 44322 Nantes, France
[3]Ecole Nationale Superieure de Chimie, de Biologie et de Physique de Bordeaux, Bordeaux INP, 33607 Pessac, France
[4]Future Industries Institute, UniSA STEM, University of South Australia, Mawson Lakes, South Australia 5095, Australia

Note: This paper is part of the Biointerphases Special Topic Collection on Biointerface Science in Australia 2020 - An issue in celebration of Hans Griesser's career.

[a)]**Author to whom correspondence should be addressed:** melanie.macgregor@unisa.edu.au

ABSTRACT

Plasma polymers derived from oxazoline precursors present a range of versatile properties that is fueling their use as biomaterials. However, coatings deposited from commonly used methyl and ethyl oxazoline precursors can be sensitive to the plasma deposition conditions. In this work, we used various spectroscopic methods (ellipsometry, x-ray photoelectron spectroscopy, and time of flight secondary ion mass spectrometry) and cell viability assays to evaluate the transferability of deposition conditions from the original plasma reactor developed by Griesser to a new wider, reactor designed for upscaled biosensors applications. The physicochemical properties, reactivity, and biocompatibility of films deposited from 2-isopropenyl-2-oxazoline were investigated. Thanks to the availability of an unsaturated pendant group, the coatings obtained from this oxazoline precursor are more stable and reproducible over a range of deposition conditions while retaining reactivity toward ligands and biomolecules. This study identified films deposited at 20 W and 0.012 mbar working pressure as being the best suited for biosensor applications.

I. INTRODUCTION

The use of plasma-enabled techniques for the creation of oxazoline-based coating was first reported in 2015 by two independent research groups.[1,2] Unlike conventional polyoxazoline polymers generated via ring opening polymerization (ROP), plasma deposited polyoxazoline (POx) films contain a variety of functional chemical groups, including intact oxazoline rings, which give them a unique reactivity toward ligands bearing carboxylic acid groups.[3,4] The use of plasma polymerization also has the advantages of being a substrate independent, solvent-free technique requiring minimal organic monomer quantities.[5,6] In contrast, other techniques for thin film deposition such as layer-by-layer and self-assembled monolayers (SAMs) require a specific substrate material and organic solvents.[7] For these reasons, plasma deposited polyoxazolines are particularly suitable for biomedical applications where the (bio)functionalization of a solid substrate is required in order to control the interaction between a biomaterial surface and the biological environment.[8] POx films have been developed for use as low fouling substrates,[2,9] biosensors,[10] and immune response modulators.[11,12]

In these works, the POx films were typically deposited from 2-methyl-2-oxazoline or 2-ethyl-2-oxazoline precursors.[2,8,13] Depending on the deposition conditions used, the resulting methyl polyoxazoline (MePOx) and ethyl polyoxazoline (EtPOx) coatings featured a variety of different physicochemical properties and reactivities. For instance, depositing MePOx at a low or high W/FM

ratio, also known as the Yasuda parameter, where W is the power input, F the precursor flow, and M the precursor molecular mass, leads to low or high fouling surfaces, respectively.[9] Similarly, different deposition parameters led to different cell growth behavior on EtPOx.[2] While the breadth of properties achievable with a single organic precursor is remarkable, MePOx and EtPOx susceptibility to deposition conditions significantly complicate transfer from one plasma deposition system to another. It also demands careful control over environmental parameters during and postdeposition as we previously demonstrated,[14] two aspects that may hinder the translation of POx into new biomedical devices and other technologies.[8]

Yet, recent works including those by Zanini *et al.* suggest that POx films with greater stability can be generated using 2--isopropenyl-oxazoline instead of the saturated methyl or ethyl monomers.[15–17] Isopropenyl polyoxazoline (PiPOx), as shown in Fig. 1(a), presents in its molecular structure an isopropenyl group in addition to the oxazoline ring, which provides more possibilities for precursor fragmentation pathways. The film forming mechanism during plasma polymerization of oxazoline-derived precursors is intrinsically different from classic ROP as it involves reactions with radicals.[18] The use of PiPOx, containing an unsaturated pendant group, has been shown to significantly increase the ring retention in films deposited using pulse plasma powers.[15] We hypothesize that not only could this improve the reactivity of the films toward COOH groups but it could also lead to more cross-linked and thus more stable films than those achieved using MePOx and EtPOx owing to the double bond available in the molecule of PiPOx that could take a significant role in the process. The resulting improvement of the POx films' reactivity and stability in relevant physiological media and/or body fluids would further expand the opportunities in developing new biomedical applications. In this work, we develop a protocol for the plasma deposition of PiPOx films with improved properties compared to MePOx for biosensor fabrication. In particular, we created a new plasma reactor with more than double the area available for the sample substrates. Transferring the deposition conditions from the Griesser reactor to this new edition and from MePOx to PiPOx, we aimed to upscale the biosensor production by 3.

We examined the effect of four different radiofrequency input powers as well as different precursor input flow rates on films generated from PiPOx in comparison to MePOx. The films' physicochemical properties, biocompatibility, and their reactivity toward appropriately functionalized nanoparticles and biomolecules were investigated via ellipsometry, x-ray photoelectron spectroscopy (XPS), time of flight secondary ion mass spectrometry (ToF SIMS), and cell viability assays. At last, we evaluated the capacity of PiPOx coatings to act as a building block for selective cell capture in biosensors. Using MePOx films as gold standard controls, we prepared PiPOx-based biosensors for the selective immunocapture of prostate cancer cells, using antiprostate specific membrane antigen (PSMA) as the capture ligand, and achieved 94% capture specificity.

II. EXPERIMENT

A. Plasma reactors and precursors

Plasma polymer deposition was performed in custom made reactors, the design of which was inspired by those originally reported by Griesser.[19] Photographs of the two designs are presented

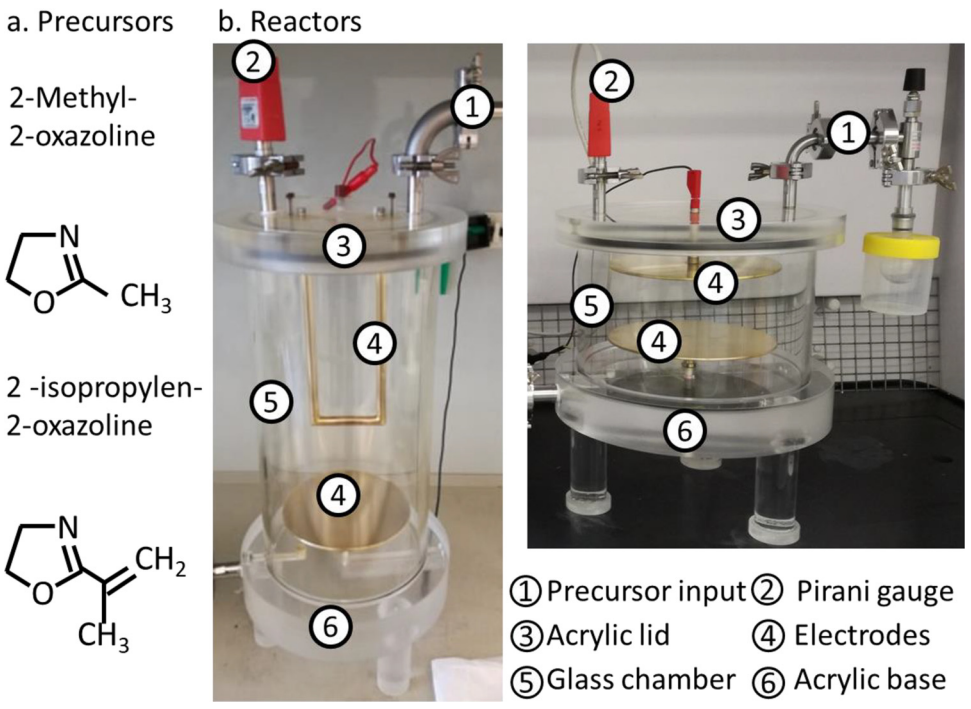

FIG. 1. (a) Precursors chemical formula. (b) Photographs of the original and new design reactors, 1 (left) and 2 (right), respectively.

in Fig. 1(b). The first one, reactor 1, has been used in previous works with oxazoline precursors.[1,3,18] The new design is herein referred to as reactor 2. This new reactor was designed to scale up the number of biosensors produced per plasma run. The result obtained in the current work from plasma depositions performed in reactor 2 will be compared to those previously obtained in reactor 1, in order to determine the parameters required to produce similar films. Both instruments consist of a tubular glass chamber resting on an acrylic base hosting a grounded circular brass electrode on which the samples are placed. In reactor 2, the diameter of the glass chamber was increased from 17 to 25 cm and that of the circular electrode from 10.3 to 18.3 cm. At the top, the reactors are both closed with an acrylic lid carrying the powered electrode, which is u-shaped in the original design and circular in reactor 2. The height of the glass chamber in reactor 2 is 15 cm, chosen to keep the overall volume of the vacuum chamber the same as in the original design of reactor 1, namely, 7.5 l. The brass electrode fittings were also designed to keep the distance between top and bottom electrode constants, 11 cm. A scaled scheme of the assembled reactor 2 is provided in Fig. S1 in the supplementary material.[39]

The plasma was ignited using a 13.56 MHz radio frequency (RF) generator coupled to a matching network (the coaxial power system). The power was varied from 10 to 50 W, according to the digital gauge of the power generator, which may differ from the actual power delivered to the electrodes because it does not correct for losses occurring along the cabling and connections. For this reason, the power read outs may not directly transfer from a reactor construction to another, and, therefore, the films generated in the new reactor 2 need to be carefully characterized to ensure that they achieve comparable performance as those created in reactor 1. Prior to the introduction of the precursor vapor, the reactors were evacuated to 2×10^{-2} mbar. The gas pressure was monitored with a pirani gauge (APG100, Edwards) and controlled with needle valves (Chell instrument, UK). The precursors, 2-methyl-2-oxazoline and 2-isopropenyl-oxazoline, were purchased from Sigma Aldrich Australia and degassed by three freeze thaw cycles with liquid nitrogen just before performing the plasma deposition. The sample substrates [silicon wafers, glass coverslips, and polymethylmethacrylate (PMMA) microchannel slides] were primed with 3 min air plasma at 1.2×10^{-1} mbar prior to plasma polymer deposition. The precursor pressure during deposition was either 1.0×10^{-1} or 1.2×10^{-1} mbar, corresponding to 4 and 7 standard cubic centimeters per minute (sccm), respectively. The deposition time was kept to 4 min for all films, as preliminary works indicated that this was appropriate to achieve the desired thickness range (data not shown). Triplicate substrates were used for all films' characterization and reactivity measurements.

B. Plasma polymer films characterization

Thickness measurements were acquired with a spectroscopic ellipsometer (J.A. Woollam, MC-200). Data were collected over the wavelength range of 400–800 nm at 65° and 75°. The thickness of the plasma polymer layer deposited onto a clean silicon wafer was determined using an established Cauchy model and fitting procedure described previously.[20] The three layer Cauchy model used to fit the data consists of an infinitely thick silicon substrate with a native oxide layer (2 nm) topped by the plasma polymer overlayer of interest. The Cauchy model is used because plasma polymer films fit the parameters of this model. The optical parameters for the silicon substrate and the native oxide layer were extracted from the modeling software library (WVASE32). The optical parameters of the plasma polymer films were refined to minimize the mean squared error of the fit and determine the films' thickness.[21] The stability of the films was evaluated by measuring film thickness loss after 1 h incubation in Milli-Q water.

XPS analysis was conducted on a Kratos Axis Ultra DLD spectrometer using a monochromatic Al Ka x-ray source operating at 225 W, which corresponds to an energy of 1 486.6 eV. The area of analysis was 0.3 by 0.7 mm. An internal flood gun was employed to minimize the charging of the samples. Survey spectra were collected at a dwell time of 55 ms with 160 eV pass energy at steps of 0.5 eV with three sweeps. The data were processed using CASAXPS (Version 2.3.16, Casa Software Ltd.).

C. POx films reactivity test

1. Reactivity toward nanoparticle ligand

The reactivity of the MePOx and PiPOx films toward ligand carrying –COOH groups was evaluated by measuring the spontaneous binding of 68 nm gold nanoparticles capped with mercaptosuccinic acid. The gold nanoparticles (AuNPs) were synthesized in house from tetrachloro auric acid ($HAuCl_4$) trisodium citrate (TSC) following well established protocols.[22–24] 400 μl of AuNPs solution was left to react for 4 h with POx-coated glass coverslips (13 mm in diameter) in 24 well plates, the solution of AuNPs was then gently aspirated, and the coverslips copiously rinsed with Milli-Q water and dried with nitrogen in preparation for XPS and scanning electron microscope (SEM) analysis.

Scanning electron micrographs were captured using SEM (Carl Zeiss Microscopy Merlin with GEMINI II column) equipped with a field-emission gun operated at 2 kV. The secondary electron images were recorded with an Evenhart Thornley secondary electron detector.

2. Reactivity with biomolecules

The reactivity of POx films toward biomolecules was evaluated by measuring the binding of antibodies and blocking proteins. ToF SIMS analysis was carried out on a PHI TRIFT V nanoTOF instrument (Physical Electronics, Inc.) with a pulsed liquid 79^+ Au primary ion gun, operated at 30 kV. Dual charge neutralization was in place in the form of an electron flood gun and Ar^+ ions (10 eV). Samples were mounted onto conductive carbon tape to avoid charging effects. Collection time per spot was 3 min, and the raster size was 10^{-4} cm^2. All spectra were processed using WINCADENCEN software (Version 1.18.1.1, Physical Electronics, Inc.) and further interrogated using NESAC/BIO ToolBox, developed at the University of Washington by Dan Graham, Ph.D.

D. Films' biocompatibility

1. Cell culture

Various human cell lines including fibroblast HFFF2 (No. 86031405), normal prostate epithelium PNT2 (No. 95012613),

prostate carcinoma LNCaP clone FGC (No. 89110211), and three types of bladder carcinoma, RT4 (No. 91091914), HT1376 (No. 87032402), and HT1197 (No. 87032403), were supplied by the European Collection of Cell Cultures (ECACC; Salisbury, United Kingdom) and purchased from CellBank Australia (Westmead, NSW, Australia). The prostate carcinoma cell line 22RV1 was provided by Dr. Luke Selth (University of Adelaide, Australia). HFFF2 cells were cultured in DMEM (Thermo Fisher Scientific, VIC Australia); RPMI-1640 media was used for PNT2, LNCaP, and 22RV1 cells; RT4 cells were maintained in McCoy's 5A media; and MEME +1% MEM nonessential amino acid solution was used for culturing HT1376 and HT1197 cells. All culture media except DMEM were obtained from Sigma Aldrich (NSW, Australia) and they were all supplemented with 10% fetal calf serum and 1% (v/v) and penicillin/streptomycin (Thermo Fisher Scientific, VIC, Australia). Cells were cultured at 37 °C in humidified atmosphere containing 5% CO_2.

2. Cell viability assay

Cells were seeded (density ~10^5 cells/ml) in 24-well plates in direct contact with the plasma deposited coating inside each well. A blank, uncoated, 24-well tissue culture plate (TCP) seeded with cells was used as control. These cells were cultured in their individual growth culture media over the material films for 24 and 48 h in order to evaluate their biocompatibility. All plates were cultured at 37 °C in humidified 5% CO_2 atmosphere.

In this study, a resazurin (alamar blue) assay was used to determine the cellular metabolic activity and mitochondrial viability of live cells. Resazurin (No. R7017, Sigma Aldrich, NSW, Australia) is a nonfluorescent dark blue indicator dye. It is reduced to resorufin, its highly fluorescent reduced form, by mitochondrial activity. The old medium was discarded after the experimental period (24 and 48 h). The fresh culture medium with 10% resazurin was added to each well. The plate was incubated at 37 °C with 5% CO_2 for 2 h. After the 2 h incubation, for each well in the plate, the total fluorescence intensity was measured using a FLUOstar OPTIMA microplate reader (BMG LABTECH, VIC, Australia), set at 540 nm excitation wavelength and a 590 nm emission wavelength. NucBlue™ Live ReadyProbes™ Reagent (Hoechst 33342) (No. R37605) from Thermo Fisher Scientific was used for cellular imaging and counting. The cells were stained with NucBlue™ for 15–30 min at room temperature according to the manufacturer's protocol. Afterward, the plate was imaged with an Olympus IX83 inverted fluorescence microscope (Japan) [Fig. 7(a)]. The number of cells in each well was counted from the nuclear stain of the fluorescent micrograph, using the automated cell count macro of the Olympus software, CELLSENS. A normalized fluorescence intensity-per-cell value was calculated for each technical replicate (n = 3) as the ratio between the total fluorescence intensity of the well (measured with the plate reader) to the number of cells in each well. For each cell line, the mean and standard deviation values were obtained from three technical replicates and used to evaluate the cell viability. Data were analyzed by MINITAB 18 software using the two-tailed unpaired student's t-test. Data were considered statistically significant at $p < 0.01$ (**) and $p < 0.001$ (***).

E. Selective cell capture

PMMA slides with three microchannels grooves were purchased from Motherson Innovations Australia[25] and six microchannel slides IV 0.4 sticky slide® from Ibidi (DSKH).[10] The microchannels were coated with a plasma deposited oxazoline thin films as described above. In reactor 1, three microchannel devices can be coated per run due to the small size of the electrode. In comparison, ten microchannel slides can be prepared in each batch run in reactor 2. This is the main motivation for optimizing reactor 2 deposition conditions as it would represent a significant upscale for the preparation of devices for clinical studies. Postdeposition, the coated microfluidic chips were kept in the dark under vacuum until further use, as established in previous aging study.[14]

1. Biofunctionalization of the polyoxazoline-coated substrate

Biofunctionalization of the microfluidic chips was performed using the protocol established in previous works.[26,27] One microchannel of the POx-coated slides is used and unmodified as a positive control (Fig. 2). The second channel was functionalized with anti-PSMA. 60 μl of anti-PSMA antibodies (10 μg/ml) was added to the microchannels and allowed to bind overnight at 4 °C. The following day, the microchannel slide was incubated at 37 °C for 1 h, before adding 1 mg/ml skim milk solution to block the anti-PSMA functionalized channel for 45 min. The last microchannel to be used as a negative control was also blocked with 1 mg/ml skim milk solution to inhibit cell binding. All the microchannels were then gently rinsed with phosphate buffered saline (PBS) three times to remove any unbound protein and fresh PBS was added.

2. Selective cancer cell capture assay

Normal prostate epithelial cells (PNT2) and prostate cancer (LNCaP) monolayer cells were trypsinized. Cancer cells were stained with 0.25 μM nuclear red and healthy cells with DAPI for 10 min. The cell densities of both cell lines were adjusted to a range between 2×10^5 and 3×10^5 cells/ml and then mixed together in 1:1 ratio. 50 μl of the mixed cell solution was pipetted into each of the three microchannels for fluorescence microscope imaging. After 45 min, unbound cells were rinsed off with 600 μl fresh PBS and the surfaces were imaged a second time. The fluorescence micrographs were used to determine the number of cells captured.[10]

III. RESULTS AND DISCUSSION

A. Physicochemical characterization

The thickness and the stability of MePOx and PiPOx films deposited in reactor 2 were evaluated via ellipsometry and are reported in Fig. 3 as a function of both RF power and precursor working pressure.

The thicknesses of the films deposited for 4 min were in the range from 24 to 34 nm for PiPOx and from 17 to 34 nm for MePOx, indicating that the PiPOx film thickness is less dependent on the deposition conditions than MePOx. For both, higher precursor pressure leads to thicker films, although the two different precursors display different deposition regimes. Indeed, for MePOx,

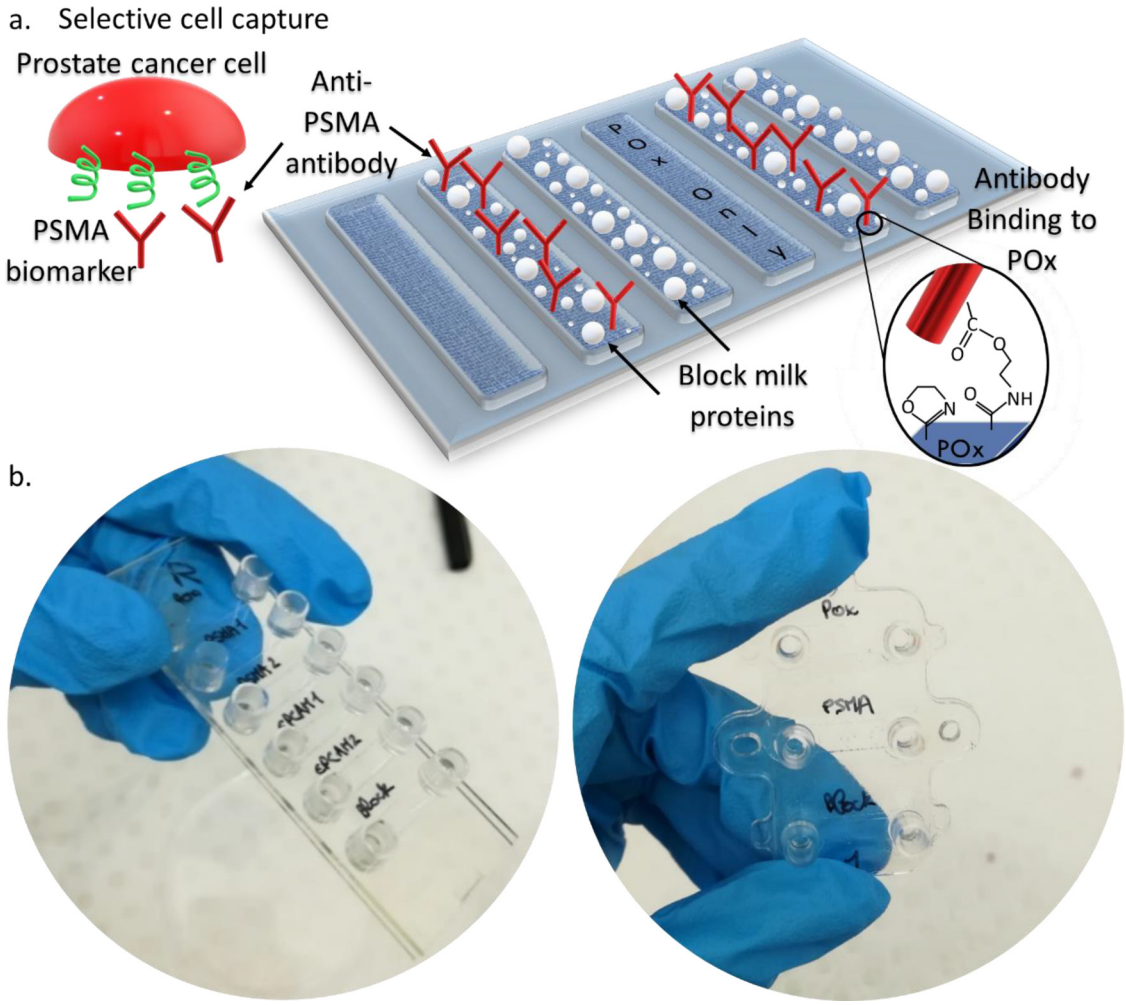

FIG. 2. (a) Schematic of the functionalized microchannel slide for cell capture experiment. (b) Photographs of the microchannel chips.

the film thickness increases with input power (W) from 10 to 20 W for a precursor pressure (F) of 1.0×10^{-1} mbar and from 10 to 30 W when the precursor pressure is increased to 1.2×10^{-1} mbar, before decreasing again at higher powers. The transition observed at 20 and 30 W for low and high precursor deposition pressure, respectively, corresponds to the shift between what has been empirically described by Yasuda as the "energy deficient" deposition regime and the "monomer deficient" regime at higher power.[28] In contrast, PiPOx films' thicknesses did not increase with input power. Instead, for both precursor pressures, as the power increases from 10 to 40 W, the film thickness decreases, indicating that the energy density is high enough to induce ion-assisted etching effects, competing with film growth processes. The only difference between the methyl and the isopropenyl-oxazoline precursor is the size and saturation level of the pendant group. The additional double bond involved in the deposition of PiPOx could lead to a greater amount of radicals in the plasma phase compared to that of MePOx. These added reactive species may contribute to the ablation process observed as the power increases and explain the difference in deposition regimes observed between PiPOx and MePOx. However, further investigations on the physics of PiPOx plasmas are warranted to test this hypothesis. Generally, films deposited with low W/F, which is in the energy deficient regime, have lower stability than those with the high W/F, monomer deficient regime, which tends to be harder and more cross linked, while functional coatings are achieved at intermediate W/F.[29] Based on the films' growth rates behavior evidenced here, functional films are expected to be created at powers below 30 W, from where etching occurs for both monomers and pressures. Below 30 W, the deposition rates of PiPOx are consistently higher than those of MePOx films.

The impact of the different deposition regimes on the stability of the films was investigated by measuring the loss in the film

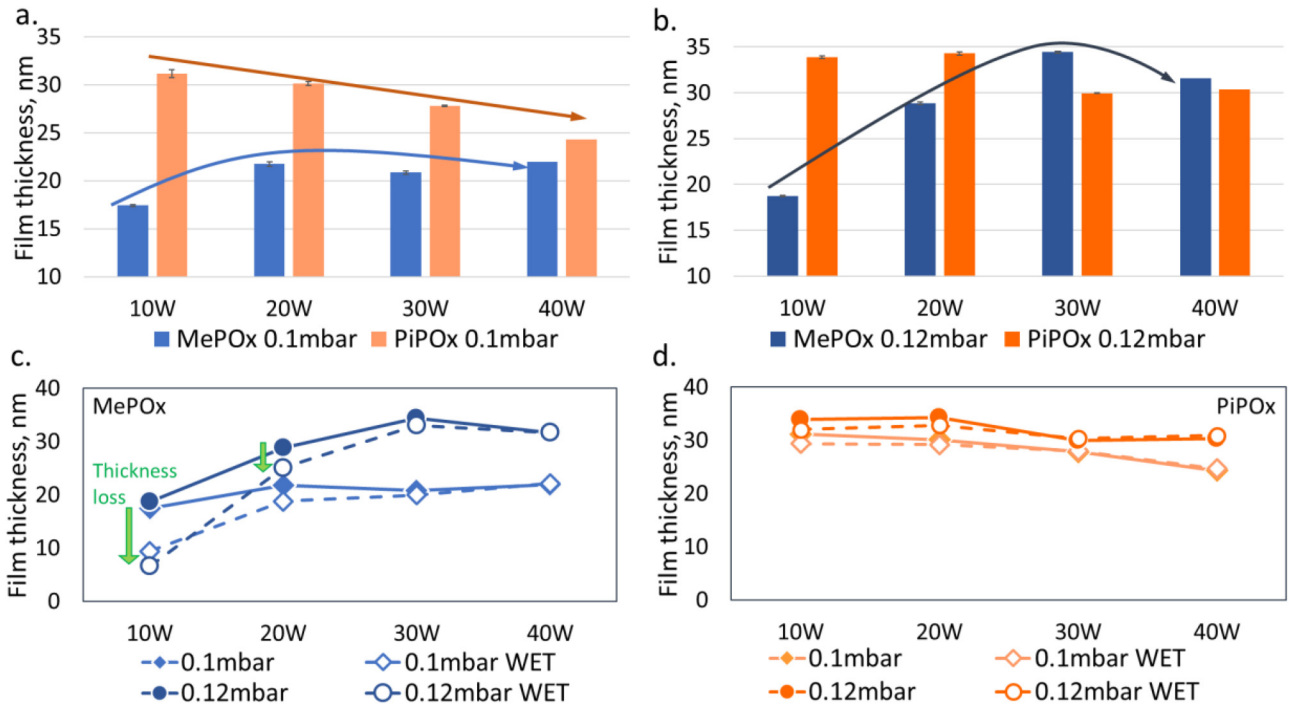

FIG. 3. Thickness (nm) of the dry POx film as a function of power (W) for MePOx and PiPOx deposited at (a) 1.0×10^{-1} and (b) 1.2×10^{-1} mbar in reactor 2 for 4 min in all films. Film thickness loss after 1 h incubation in water for (c) MePOx and (d) PiPOx.

thickness after 1 h incubation in Milli-Q water [Figs. 3(c) and 3(d)]. Before water exposure, for both MePOx and PiPOx, the films were thicker when deposited with the highest precursor pressure, though the difference was more significant for MePOx with an increase of up to 15 nm observed at 30 W. After water exposure, however, the MePOx films suffered substantial thickness loss of up to 65% for the film with the lower W/F factor deposited at 10 W and 1.2×10^{-1} mbar working pressure. For MePOx films to suffer less than 10% thickness loss, the deposition in reactor 2 must be carried out with an ignition power above 20 W. In comparison, MePOx films deposited in reactor 1 at a comparable working pressure (8 sccm) lose more than 95% of their thickness when deposited at 10 W and still above 20% when deposited at 50 W, as previously reported.[3] When deposited at 4 sccm in reactor 1, MePOx films stood a 20% loss at 10 W and less than 10% from 30 W onward.[9] The MePOx films deposited in reactor 2 are, therefore, no less stable than those deposited in reactor 1. In contrast, all PiPOx films deposited in reactor 2 were stable with insignificant thickness losses or gain over the range of conditions investigated. Overall, the PiPOx films appeared to be more stable than those deposited from MePOx, less sensitive to the deposition conditions, and faster to deposit at low W/F. These characteristics of the plasma deposited films can only be attributed to the presence of an unsaturated pendant group on the PiPOx precursors since all other aspects were kept constant between the two monomers. Previous studies investigating the effect of unsaturation on the mechanisms of plasma polymer depositions and also found that unsaturated monomers deposit faster than their saturated analogs at low powers.[30,31] This was attributed to films' growth occurring by neutral grafting of radicals through the fragmentation of the unsaturated group, as opposed to being predominantly an ionic process for saturated monomers. The difference in the film growth mechanism may also explain the increase in film stability for PiPOx. In addition to the ionic mechanism occurring for both monomers, PiPOx provides additional radical sites for postadsorption rearrangement via radical propagation toward the lowest thermodynamic conformation.[31] The rearrangement of the bulk of the polymer films into stable configurations occurs postdeposition. It can, therefore, stabilize films deposited at low powers, where ionic processes fail to create strong cross-links.

The atomic composition of the POx films was investigated via XPS. Representative survey spectra are provided in Fig. S2 in the supplementary material,[39] and Fig. 4 shows the elemental composition analysis in terms of nitrogen content and heteroatom ratio to carbon, N/C and O/C. The nitrogen content of the POx film arises from the presence of amine, amide, imine chemical groups, and intact oxazoline rings.[3,18] The nitrogen content, N %, therefore, provides an indirect evaluation of the film functionality. The PiPOx films contain less nitrogen (9%–11%) than the MePOx films (9%–15%) at all deposition conditions investigated in the new design reactor 2. This is in good agreement with the composition of the intact precursor chemical structure, which is represented with the

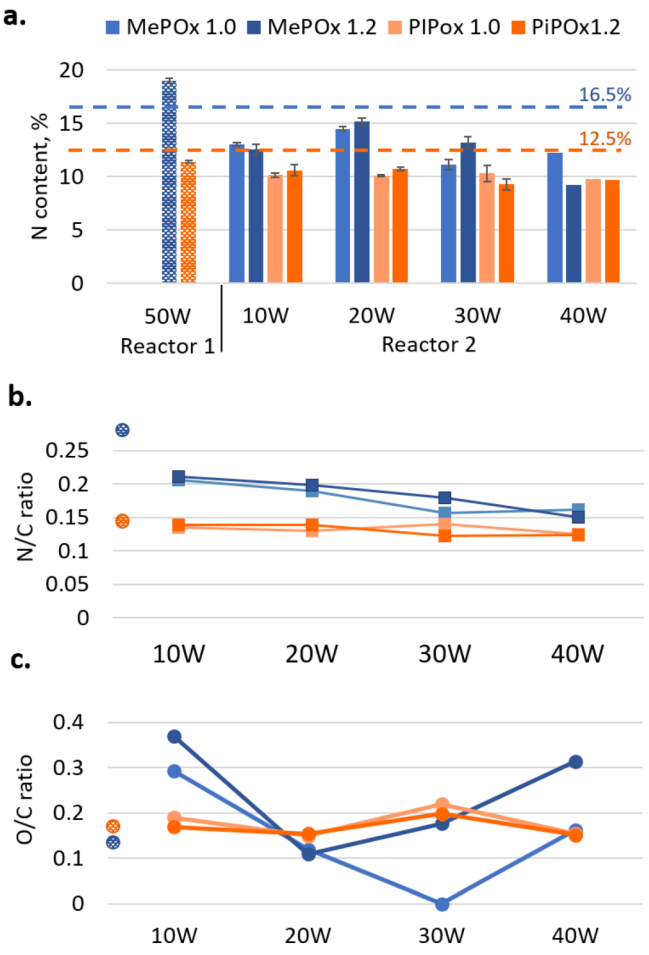

FIG. 4. Atomic content analysis from XPS survey spectra of POx films deposited for 4 min. (a) N%, (b) nitrogen on carbon ratio, and (c) oxygen on carbon ratio.

dotted blue and orange lines in Fig. 4(a) for MePOx (16.5% N) and PiPOx (12.5% N), respectively. It is worth noting, however, that for MePOx deposited in the original reactor (reactor 1) and in optimized conditions (50 W, 1.2×10^{-1} 0.12 mbar), a nitrogen content above that of the monomer itself and as high as 19% was achieved, which resulted in high N/C ratio [Fig. 4(b), a round marker indicates the ratio for the film deposited in the original reactor 1 conditions from Ref. 14]. This, particularly, high nitrogen content has been attributed to the vacuum depletion of small, volatile oxygenated species such as CO or CO_2 during deposition[32] and is supported here by the trend observed in the O/C ratio shown in Fig. 4(c). Indeed, for MePOx, the O/C ratios are lower when the deposition occurred at 1.0×10^{-1} mbar precursor pressure compared to films deposited at 1.2×10^{-1} mbar, indicating that oxygen-rich species are sparse in the "monomer deficient" deposition regime. In reactor 2, the nitrogen content is systematically below that of the corresponding monomer, indicating that small nitrogen-containing fragments may also be pumped out of the reaction chamber during deposition, as previously reported for sulfur-rich plasma polymers.[33] While the N % is rather constant for PiPOx films, it reaches a maximum of 15% for MePOx deposited at 20 W, that is, the intermediate zone between the two deposition regimes observed through ellipsometric analysis. The susceptibility of the MePOx film heterofunctionality to deposition conditions is further confirmed by the N/C and O/C analysis. For instance, the O/C ratio displays a clear minimum at 20 W for 1.2×10^{-1} mbar precursor working pressures and at 30 W for 1.0×10^{-1} mbar. In contrast, the atomic composition and heteroatom ratio for PiPOx display little variation from the original monomer composition and across all reactors deposition conditions investigated. However, the fact that PiPOx films contained less heteroatoms than MePOx does not necessarily mean that their surface is less rich in reactive functionalities, such as intact oxazoline rings. In fact, the volatile species that are pumped out during deposition are likely to consist of small stable molecules (e.g., CO, CO_2, NO, and HCN), which would not contribute to the film reactivity. In order to test this hypothesis, the POx film reactivity toward ligands bearing acrylic acid functionality was investigated.

B. Films' reactivity

In order to assess the reactivity of the POx films toward ligands bearing carboxylic acid chemical groups, the films were incubated with gold nanoparticles (AuNPs) capped with mercaptosuccinic acid (Fig. 5). XPS survey spectra were recorded after incubation in the AuNPs solution for 4 h to measure the amount of atomic gold bound to the substrates. AuNPs spontaneously bound to both MePOx and PiPOx films. However, on MePOx films deposited at the lowest power, 10 W, the atomic percentage of gold recorded was below 1% with effectively no gold found on those deposited at 1.2×10^{-1} mbar. On these coatings, which are also the least stable, the partial dissolution of the films hinders AuNPs binding. In contrast, the nanoparticles did bind to the PiPOx films deposited at 10 W.

At 30 and 40 W, films prepared from both precursors consistently bound between 1.5% and 2.5% of gold with negligible variation between the two deposition pressures investigated. This amount is comparable to that reported on MePOx films deposited in reactor 1.[34] The maximum AuNPs adsorption was recorded on the films deposited at 20 W for both precursors. However, at this power, large variations are seen within each deposition pressure conditions, especially for MePOx, where the gold atomic content ranges from 1% to 3.5%, depending on the location of the sampling spot measured via XPS. These results are in good agreement with a macroscopic observation of the coverslips color made during the incubation steps. Indeed, the plasmon resonance phenomenon gives monodisperse AuNPs, a coloration ranging from light to dark pink as their size increases. This coloration is visible on the otherwise transparent glass coverslips in Fig. 5(b), for AuNPs in solution (top well) and bound to PiPOx films (bottom well). In Fig. 5(c), however, one can see that a color change toward purple or even gray occurred on the MePOx films deposited in the same conditions (20 W, 1.2×10^{-1} mbar). This color change is due to the larger size of the colloidal entities present both in suspension and

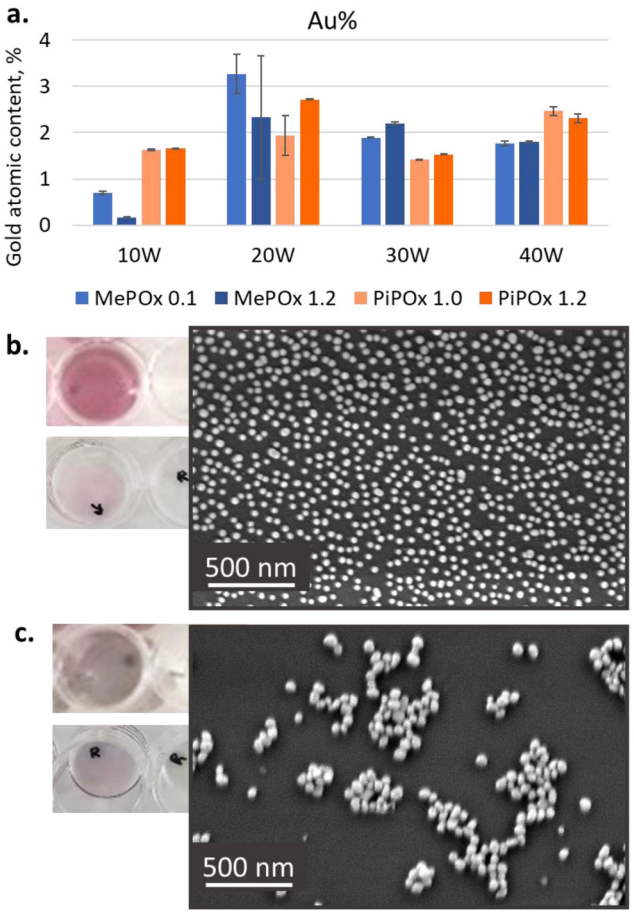

FIG. 5. POx film reactivity tests with a gold nanoparticle. (a) XPS data of the gold atomic content in per cent following 4 h incubation with 68 nm gold nanoparticles, (b) corresponding SEM images and well plate photograph for PiPOx, and (c) for MePOx deposited at 20 W and 1.2×10^{-1} mbar for 4 min.

bound to the coverslip, indicating aggregation. To further interrogate this phenomenon, SEM images were acquired for both MePOx and PiPOx deposited at 20 W with 1.2×10^{-1} mbar deposition pressure [Figs. 5(b) and 5(c)]. The micrographs confirmed that aggregation occurred on the MePOx films, while nanoparticles adhered as individual entities on the PiPOx films. The fact that the AuNPs solution itself displayed a gray coloration in the MePOx well indicates that aggregation occurred in solution. This suggests that chemical species eluting from the poorly stable MePOx films destabilized the colloidal suspension. Previous reports have also flagged that although MePOx films deposited at low powers had higher reactivity toward COOH-bearing ligand, this advantage could not be exploited further because of the poor film stability associated with these deposition conditions.[3] This phenomenon is expected to become particularly detrimental for functionalization with biomolecules, as proteins could undergo denaturation upon exposure to the chemical elutions from the MePOx film. Denatured biomolecules lose their biofunctionality. For antibodies, this results in a loss of specificity toward their target antigens, typically making the biofunctionalization pointless for use in biosensors. The results shown here for PiPOx films open up new possibilities for the use of POx films deposited at low power featuring both enhanced reactivity and satisfactory stability.

The reactivity of MePOx and PiPOx films toward biomolecules was assessed via ToF SIMS. For these experiments, the POx films were allowed to react with the same antibody and blocking agents as those used to produce the selective cell capture biosensor platform, namely, anti-PSMA antibodies and skim milk proteins.[25]

ToF SIMS is a highly sensitive technique that detects low molecular weight fragments present in the top 2 nm of the surface investigated. It is a method of choice for the analysis of complex nanothin films such as self-assembled monolayers,[35] plasma polymers,[36] and surface adsorbed antibodies[37] because of its very high mass resolution. Overall, MePOx and PiPOx have very similar surface chemistry, as seen from the positive fragment spectra shown in Fig. S3 in the supplementary material.[39] Nonetheless, principal component analysis (PCA) revealed that they can be statistically differentiated. PCA is a multivariate statistical analysis used for the interpretation of complex multidimensional datasets. It enables the visualization of the greatest variance across the dataset. PCA of the ToF SIMS data was used to identify which specific molecular fragments distinguished PiPOx from MePOx and subsequently, pristine POx films from biofunctionalized ones. The first and second greatest variances are referred to as principal component PC1 and PC2 and plotted in Fig. 6(a). PC1 and PC2 accounted for 95% of the total variance in the MePOx versus PiPOx dataset. In the resulting bidimensional plane, the two coatings are well clustered and their 95% confidence interval (CI) area does not overlap, thus demonstrating distinct chemical signatures. The 95% CI area is larger and more diffuse for MePOx than for PiPOx, which indicates a lesser reproducibility across the different spots tested, as expected from the variability issues already identified via ellipsometry and XPS. Analysis of the PC1 loadings for the different polymer fragments [Fig. 6(b)] shows that at the surface layer, MePOx and PiPOx differ in terms of labile group size (m/z) and functionality. Compared to PiPOx, the top-most surface of MePOx contains more large fragments containing both O and N heteroatoms than PiPOx. These include the nitrile species CH_2N+ at m/z 28, C_2H_4N+ with $m/z = 42$, and C_3H_6N+ with $m/z = 56$, as well as aldehyde C_2H_3O+ at $m/z = 43$ and also the oxazoline ring itself at $m/z = 72$ and the methylated oxazoline ring at $m/z = 86$. These surface functional groups originate from different fragmentation pathways occurring in the plasma phase and recombination reactions occurring postdeposition, as previously described.[18] They are not present in "classic" polyoxazoline polymerized via conventional organic chemistry methods and are, therefore, intrinsic to the unique reactivity of plasma deposited POx films. In contrast, PiPOx contained more small carbon rich fragments with $m/z < 30$. Nonetheless, both films markedly bound antibodies, as evidenced from the principal component analysis in Fig. 6(c). The distinct scoring of the 95% CI for both PiPOx and MePOx across the PC2 axis confirms the success of the two biofunctionalization steps, namely, antibody binding then blocking with skim milk. Typically, the first step of PCA analysis for a protein surface is to include all

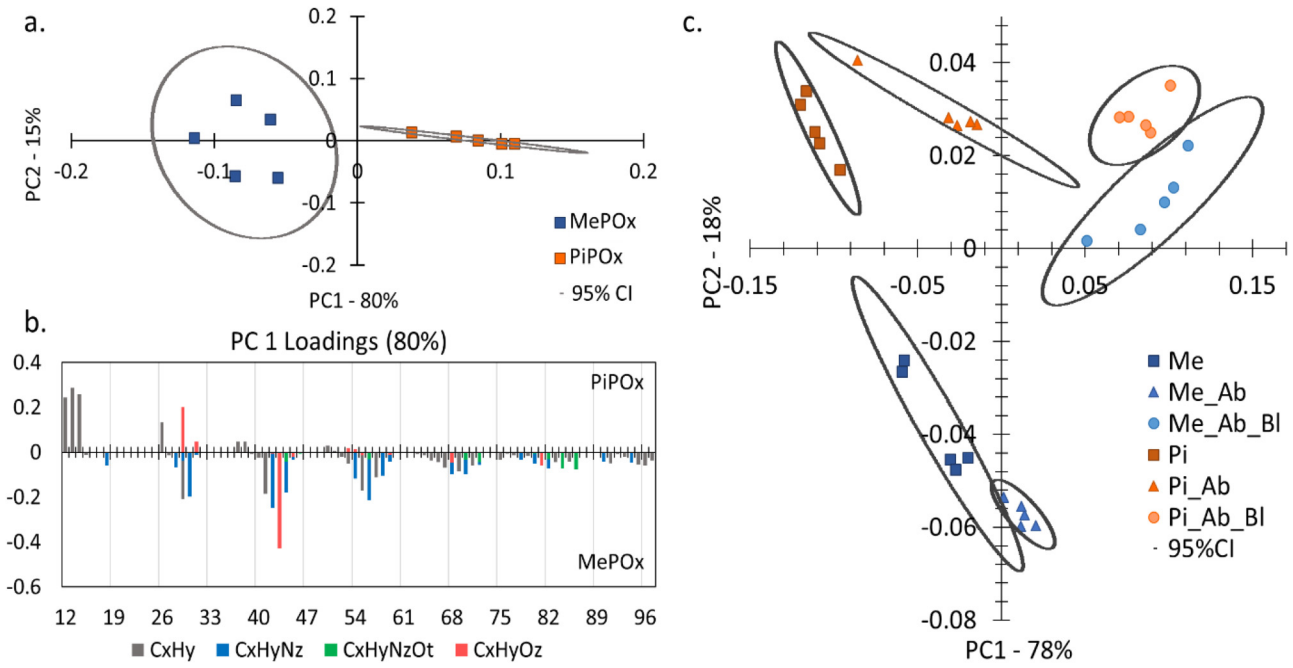

FIG. 6. ToF SIMS analysis. (a) Principal component analysis loading for pristine MePOx and PiPOx. (b) PC1 loading for all fragments below 100 m/z. PiPOx fragments load in the positive direction and MePOx fragments in the negative direction. (c) PCA scores plot for PC1 and PC2 from ToF SIMS data for the POx films biofunctionalization steps with antibodies (triangles) and block proteins (circles). PC2 distinguishes the different substrate compositions (i.e., PiPOx vs MePOx), while PC1 (78%) separates the biofunctionalization steps.

amino acid fragments to the analysis.[38] This is complicated in the case of POx coatings because the underlying substrate produces interfering peaks at similar m/z, which also contains nitrogen and oxygen atoms. Nonetheless, PCA identified fragments corresponding to the biomolecules in statistically higher amount after incubation with the anti-PSMA than beforehand. Specifically, fragments, such as C_4H_8N+ corresponding to proline and valine, $C_4H_{10}N+$ corresponding to valine, $C_5H_{10}N+$ corresponding to lysine and leucine, and $C_5H_{12}N+$ corresponding to both leucine and isoleucine, were identified on the protein coated surfaces, as shown in Fig. S4 in the supplementary material.[39]

When blocking protein was added to the substrate, the film surface chemistry changed again as seen from the lack of overlap between 95% CI area between MePOx and MePOx + AB and also between PiPOx and PiPOx + AB. However, the CI for the two biofunctionalized plasma polymer substrates is brought closer together following the blocking step. This is because the blocking layer is thicker than the ToF SIMS analysis depth. As a result, the block proteins screen the effect of the underlying POx layer. The top 2 nm essentially reflect the chemical signature of the antibody and block protein, which has no reason to differ from MePOx to PiPOx unless the proteins are orientated in a preferential way on one of the plasma polymers.

Overall, these results indicate that despite their lower nitrogen content, the PiPOx films are as reactive as their MePOx counterpart, effectively binding COOH-bearing ligand spontaneously at room temperature in Milli-Q water and biological buffer. PiPOx reactivity comes with two advantages over MePOx. First, the PiPOx films deposit faster and are more stable than MePOx at low deposition power. Second, they are more tolerant to deposition conditions. For these two reasons, PiPOx is potentially more reliable for the spontaneous binding of functional biomolecules. This hypothesis was tested in Sec. II E, where MePOx and PiPOx films were used to build biosensors for the selective capture of prostate cancer cells.

C. Films' biocompatibility

Seven different human cell lines including noncancer prostate PNT2, prostate cancer LNCaP and 22RV1, normal fibroblast HFFF2, and bladder carcinoma HT1376, HT1197, and RT4 were used to analyze the cytotoxicity of PiPOx and MePOx deposited at 20 W with 1.2×10^{-1} mbar working pressure, after 24 and 48 h cell growth period, as schematized in Fig. 7(a). The fluorescence intensity per cell was calculated to determine the cell viability [Figs. 7(b) and 7(c)]. Absolute cell numbers are provided in Figs. S5(a) and S5(b) in the supplementary material.[39] After 24 h incubation on the PiPOx film, the cell viability was higher than on the control TCP control in most cell lines. Indeed, the live-dead staining showed that the cells have higher fluorescence on PiPOx coated plates than TCP, indicating that PiPOx is biocompatible, Fig. 7(d). The increase in fluorescence normalized to the absolute cell

number was significant for PNT2 and HT1376 with $p < 0.001$ and $p < 0.05$, respectively. After 48 h, the increase was significant for 22RV1 and RT4. In contrast, there was more variability in the cell viability on MePOx coated plates. The biocompatibility at 24 h was only significantly higher for PNT2, and at 48 h, it was higher for RT4, which was as significant as that for PiPOx.

In both cases, the average of the normalized fluorescence is lower on PiPOx and MePOx than on TCP for LnCap cells. This is, however, due to the cells clumping on the TCP, which results in a large deviation from one biological replicate to the other. In contrast, the LnCap cells formed homogeneous monolayers on the POx-coated plates, as shown in Fig. S6 in the supplementary material.[39]

It is worth noting that MePOx coatings deposited at higher powers in the original reactor were consistently biocompatible for a variety of cell lines, namely, human dermal fibroblasts,[3] macrophages,[11] and colon cancer cells and podocytes.[10] The variability observed here for films deposited at 20 W could, therefore, be attributed to the poor stability of the film-releasing chemicals, which may affect some cell lines more than others. These results indicate that, overall, cell proliferation is not hindered on PiPOx or MePOx substrates prepared in the new reactor 2.

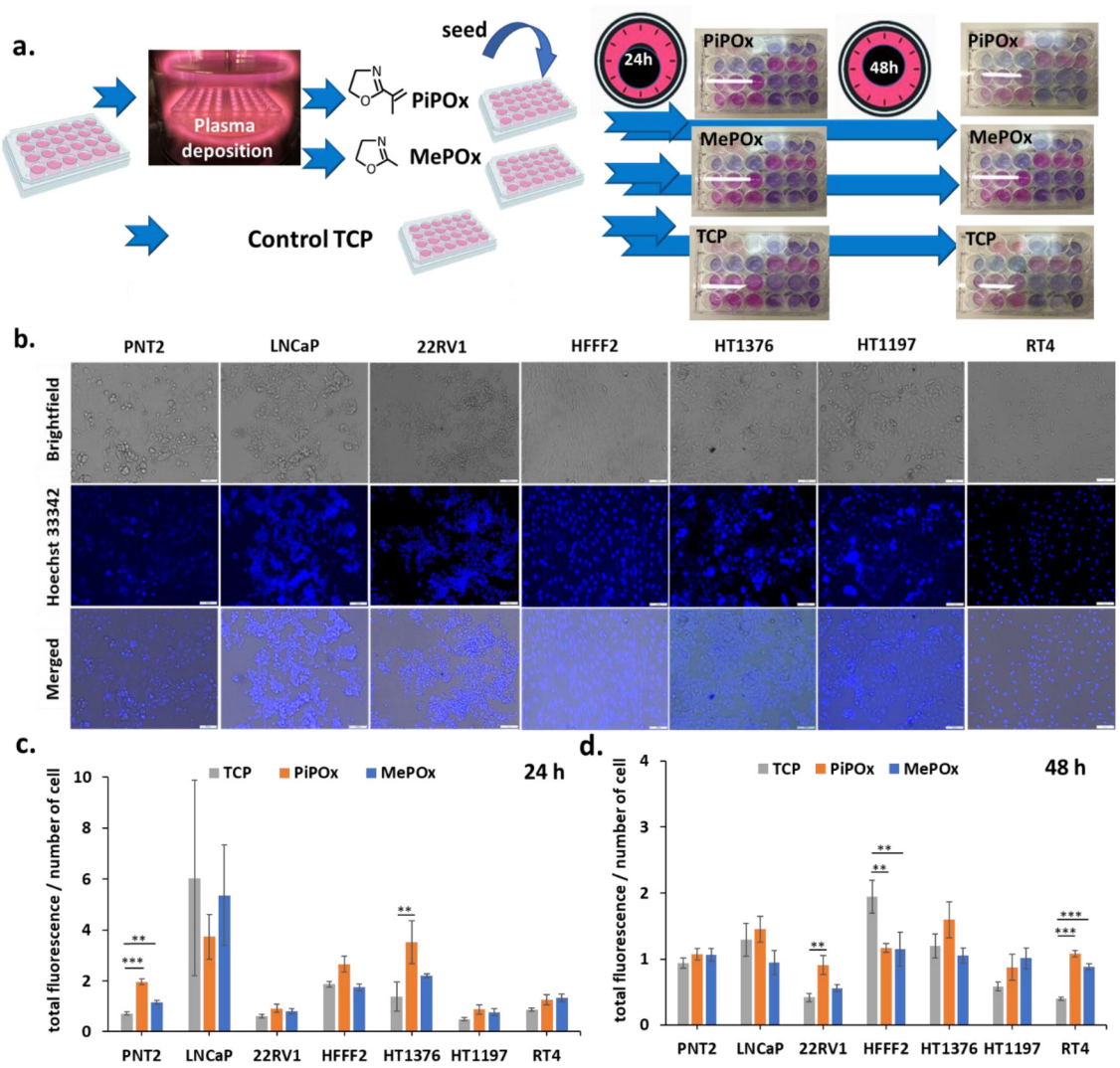

FIG. 7. Cell viability on PiPOx and MePOx. (a) Schematic of the experiment design; (b) microscopic images of NucBlue stained PNT2, LNCaP, 22RV1, HFFF2, HT1376, HT1197, and RT4 cells which cultured on PiPOx coated plate after 24 h. Scale bar: 200 μm; the total resorufin fluorescence intensities-to-number of cell ratio of monolayer cells (n = 3) cultured in TCP compared to PiPOx and MePOx after (c) 24 h and (d) 48 h. Mean ± standard derivation, $^{**}p < 0.01$, $^{***}p < 0.001$.

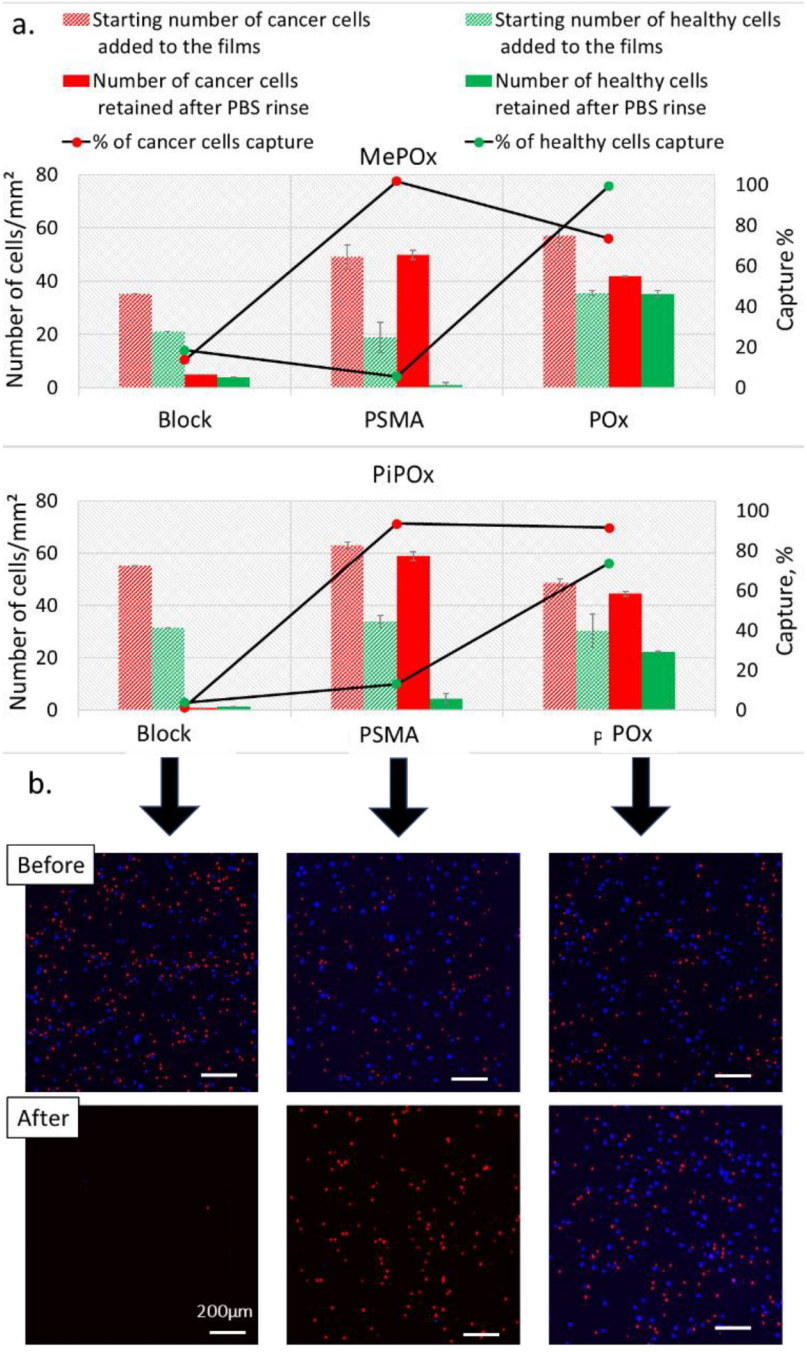

FIG. 8. Selective cell capture assay. (a) Cell capture absolute numbers (the left axis) and capture rates in per cent (the right axis) for control block channels, PSMA bio-functionalized channel, and pristine MePOx (top) or PiPOx (bottom). (b) Representative micrograph of the cells present in PiPOx channels. Normal prostate cells (PNT2) are stained in blue, and cancerous prostate cells are stained in red.

D. PiPOx film for selective cell capture biosensors

In order to test the biofunctionality of antibodies bound to the PiPOx substrates, biosensors for the selective capture of prostate cancer cells were prepared. The microfluidic chips contained three channels, namely, one coated with pristine POx, as a positive control onto which all cell types bind in a nonspecific manner. One functionalized with anti-PSMA antibodies. PSMA is a prostate cancer specific biomarker situated on the membrane of prostate cancer cells. In preliminary works performed on the original reactor 1, we demonstrated the ability of MePOx coated microchannels functionalized with anti-PSMA to selectively bind prostate cancer cells with a selective capture rate up to 97% sensitivity.[25]

The last channel is blocked with skim milk protein and used as a negative control, where minimal cell binding is expected. The results from the cell capture experiment performed using MePOx and PiPOx deposited in reactor 2 at 20 W with 1.2×10^{-1} mbar working pressure are shown in Fig. 8. Low cell numbers remained bound to the block channels after PBS rinse. For PiPOx, less than 4% of cells bound to the block substrate. However, on the blocked MePOx channel, up to 18% of cells remained bound to the negative control. This could be due to lower or patchy adhesion of the skim milk protein to the MePOx film. The pristine MePOx and PiPOx channels captured both cell types nonspecifically, as expected from this positive control substrate. However, the capture rate recorded was as low as 73% for normal prostate cells on PiPOx or cancer cells on MePOx. This is somewhat lower than what is achieved on MePOx films deposited with optimized deposition conditions in the original reactor 1, where the nonselective capture of both cell types is typically above 90%, as we just reported.[25,26] It could be attributed to the lower amount of nitrogen-containing chemical groups on the POx films generated in reactor 2, as amines are known to facilitate cell adhesion. In the test channel functionalized with anti-PSMA, however, selective prostate cancer cell capture is observed for both MePOx and PiPOx substrates with capture rates of 95% and 94%, respectively, which is comparable to what is achieved from MePOx films deposited in reactor 1 (up to 97%). The anti-PSMA antibodies bound to both POx surfaces through reaction with carboxylic acid groups have retained their bioactivity. Overall, the results demonstrate that PiPOx films deposited in the new reactor design, at 20 W with 1.2×10^{-1} mbar precursor working pressure can be used to create biosensors for selective cell capture, as illustrated in the micrograph in Fig. 8(b).

IV. SUMMARY AND CONCLUSIONS

The properties of plasma deposited polyoxazoline films can be useful to the development of biomaterials and coatings for the biomedical industries. However, films deposited from methyl-2-oxazoline are very susceptible to variation in film deposition conditions and environmental factors, which hinders translation from one plasma setting to another. Here, we showed that films deposited from isopropenyl-oxazoline are less sensitive to the deposition conditions than those deposited from methyl-2-oxazoline. They were successfully prepared in a new upscaled reactor allowing higher throughput of samples. In the range of power investigated, from 10 to 40 W, the PiPOx films are stable, reproducible, and yet still reactive. The PiPOx films successfully bound both gold nanoparticles and biomolecules. At last, the PiPOx films are biocompatible and antibodies binding their surface remain bioactive enough to selectively capture a cell population of interest with 94% efficiency. The films developed here are promising candidates for the development of biosensors.

ACKNOWLEDGMENTS

The authors acknowledge the instruments and scientific and technical assistance of Microscopy Australia at the Future Industries Institute, University of South Australia, a facility that is funded by the University, and State and Federal Governments. M.M. and K.V. acknowledge the ARC research council for DP180101254 and the CRC-P program for funding. M.M. acknowledges the UniSA RTIS grant scheme. M.M. acknowledges the support of the University of South Australia/University College London-Santos Fellowship.

REFERENCES

[1]M. N. Ramiasa, A. A. Cavallaro, A. Mierczynska, S. N. Christo, J. M. Gleadle, J. D. Hayball, and K. Vasilev, Chem. Commun. **51**, 4279 (2015).
[2]S. Bhatt, J. Pulpytel, M. Mirshahi, and F. Arefi-Khonsari, Plasma Process. Polym. **12**, 519 (2015).
[3]M. N. Macgregor-Ramiasa, A. A. Cavallaro, and K. Vasilev, J. Mater. Chem. B **3**, 6327 (2015).
[4]S. Zanini, L. Zoia, E. C. Dell'Orto, A. Natalello, A. M. Villa, R. D. Pergola, and C. Riccardi, Mater. Des. **108**, 791 (2016).
[5]K. Vasilev, A. Michelmore, H. J. Griesser, and R. D. Short, Chem. Commun. **2009**, 3600.
[6]K. Vasilev, A. Michelmore, P. Martinek, J. Chan, V. Sah, H. J. Griesser, and R. D. Short, Plasma Process. Polym. **7**, 824 (2010).
[7]J. L. Hernandez-Lopez *et al.*, Mater. Sci. Eng. C **23**, 267 (2003).
[8]M. Macgregor and K. Vasilev, Materials **12**, 191 (2019).
[9]A. A. Cavallaro, M. N. Macgregor-Ramiasa, and K. Vasilev, ACS Appl. Mater. Interfaces **8**, 6354 (2016).
[10]M. Macgregor-Ramiasa, K. McNicholas, K. Ostrikov, J. Li, M. Michael, J. M. Gleadle, and K. Vasilev, Biosens. Bioelectron. **96**, 373 (2017).
[11]R. M. Visalakshan *et al.*, ACS Appl. Mater. Interfaces **11**, 27615 (2019).
[12]Z. Chen, R. M. Visalakshan, J. Guo, F. Wei, L. Zhang, L. Chen, Z. Lin, K. Vasilev, and Y. Xiao, Acta Biomater. **96**, 568 (2019).
[13]S. A. Al-Bataineh, A. A. Cavallaro, A. Michelmore, M. N. Macgregor, J. D. Whittle, and K. Vasilev, Plasma Process. Polym. **16**, 1900104 (2019).
[14]M. MacGregor, U. Sinha, R. M. Visalakshan, A. Cavallaro, and K. Vasilev, Plasma Process. Polym. **16**, 1800130 (2019).
[15]S. Zanini, L. Zoia, R. Della Pergola, and C. Riccardi, Surf. Coat. Technol. **334**, 173 (2018).
[16]S. Zanini, M. Lehocky, J. Lopez-Garcia, and C. Riccardi, Thin Solid Films **677**, 55 (2019).
[17]M. C. MacGregor-Ramiasa, A. Visalakshan, R. M. L. Gonzalez, and K. Vasilev, in *Chemeca 2016: Chemical Engineering—Regeneration, Recovery and Reinvention* (Engineers Australia, Adelaide, 2016), pp. 302–312.
[18]M. N. Macgregor, A. Michelmore, H. Safizadeh Shirazi, J. Whittle, and K. Vasilev, Chem. Mater. **29**, 8047 (2017).
[19]H. J. Griesser, Vacuum **39**, 485 (1989).
[20]A. M. Sandstrom, M. Jasieniak, H. J. Griesser, L. Grøndahl, and J. J. Cooper-White, Plasma Process. Polym. **10**, 19 (2013).
[21]S. Saboohi, B. R. Coad, A. Michelmore, R. D. Short, and H. J. Griesser, ACS Appl. Mater. Interfaces **8**, 16493 (2016).
[22]R. M. Visalakshan, M. N. MacGregor, A. A. Cavallaro, S. Sasidharan, A. Bachhuka, A. M. Mierczynska-Vasilev, J. D. Hayball, and K. Vasilev, ACS Appl. Nano Mater. **1**, 2796 (2018).
[23]S. Taheri, J.-C. Ruiz, A. Michelmore, M. Macgregor, R. Förch, P. Majewski, and K. Vasilev, J. Phys. Chem. C **122**, 14986 (2018).
[24]R. M. Visalakshan, A. A. Cavallaro, M. N. MacGregor, E. P. Lawrence, K. Koynov, J. D. Hayball, and K. Vasilev, Adv. Funct. Mater. **29**, 1807453 (2019).
[25]H. S. Shirazi *et al.*, Biointerphases **15**, 031002 (2020).
[26]K. M. Chan, K. Vasilev, H. S. Shirazi, K. McNicholas, J. Li, J. Gleadle, and M. Macgregor, Photodiagn. Photodyn. Ther. **28**, 238 (2019).
[27]K. Ostrikov, T. Michl, M. MacGregor, and K. Vasilev, ACS Appl. Bio Mater. **2**, 3730 (2019).
[28]H. Yasuda, *Plasma Polymerization* (Academic, New York, 1985).
[29]D. Hegemann, in *Comprehensive Materials Processing*, edited by S. Hashmi, G. F. Batalha, C. J. Van Tyne, and B. Yilbas (Elsevier, Oxford, 2014), pp. 201–228.

[30]D. Barton, A. G. Shard, R. D. Short, and J. W. Bradley, J. Phys. Chem. B **109**, 3207 (2005).
[31]A. Michelmore, D. A. Steele, D. E. Robinson, J. D. Whittle, and R. D. Short, Soft Matter **9**, 6167 (2013).
[32]S. Saboohi, B. R. Coad, H. J. Griesser, A. Michelmore, and R. D. Short, Phys. Chem. Chem. Phys. **19**, 5637 (2017).
[33]E. Kasparek, D. Thiry, J. R. Tavares, M. R. Wertheimer, R. Snyders, and P.-L. Girard-Lauriault, Plasma Processes Polym. **15**, 1800036 (2018).
[34]L. Gonzales-Garcia, M. Macgregor-Ramiasa, and K. Vasilev, "Protein interactions with nanoengineered polyoxazoline surfaces generated via plasma deposition," Langmuir **33**(29), 7322–7331 (2017).
[35]M. Holzweber, T. Heinrich, V. Kunz, S. Richter, C. H. H. Traulsen, C. A. Schalley, and W. E. S. Unger, Anal. Chem. **86**, 5740 (2014).
[36]A. J. Ward and R. D. Short, Polymer **36**, 3439 (1995).
[37]N. G. Welch, R. M. T. Madiona, T. B. Payten, C. D. Easton, L. Pontes-Braz, N. Brack, J. A. Scoble, B. W. Muir, and P. J. Pigram, Acta Biomater. **55**, 172 (2017).
[38]F. Liu, M. Dubey, H. Takahashi, D. G. Castner, and D. W. Grainger, Anal. Chem. **82**, 2947 (2010).
[39]See the supplementary material at http://dx.doi.org/10.1116/6.0000499 for reactor 2 engineering scheme, XPS full spectra, detailed ToF SIMS and cell viability study.